Modeling Fiber-Like Conductivity Structures via the Boundary Element Method Using Thin-Wire Approximation. I Construction of Basis Functions

Sergey N Makarov[1], *Senior Member, IEEE*, Alvaro Pascual-Leone[2], and Aapo Nummenmaa[3]

***Abstract*— A set of one-dimensional basis functions is proposed and tested in order to model a thin homogeneous fiber of a higher conductivity within a medium with a lower conductivity. This set allows us to greatly speed up computations while keeping a good accuracy for the total fiber current and the resulting charge distribution averaged over the fiber cross-section.**

I. Introduction

Anatomically realistic modeling of different conductivity structures is important for noninvasive brain imaging and stimulation, including electro- and magnetoencephalography, (E/MEG), transcranial magnetic stimulation (TMS), and transcranial direct/alternating current stimulation (tDCS/tACS) [1]-[5]. An important example is given by bundles of a conducting fibers (*e.g.*, axons) located in a conducting medium. Although the problem might be solved using an average anisotropic conductivity tensor, this method is not without its limitations. For instance, crossing fibers might generate an anisotropic conductivity structure that is not described by a tensor. A significantly more flexible approach will be considered in this study, which enables modeling individual fibers in a "thin-wire" approximation, using certain one-dimensional BEM (Boundary Element Method or MoM – Method of Moments) basis functions. We show that a small number of such basis functions is sufficient to accurately describe current and average charge distribution for any fiber cross-section. Although the proposed method is general, only straight fiber of a fixed radius is considered in the present study, for steady-state current flow problems.

II. Basis Functions and Governing Equations

First, consider a simple modeling problem shown in Fig. 1. A relatively thin cylinder with the radius a of 1 mm, length L of 40 mm, and conductivity of 4 S/m is embedded into a homogeneous conducting medium with a smaller conductivity of 0.5 S/m. An external uniform electric field $\mathbf{E}_{\text{inc}}$ of 10 V/m is applied, which excites currents both in the medium and in the cylinder. Fig. 1 shows surface charge and current density distributions, respectively, in the cylinder plane obtained via FEM modeling with Maxwell 3D of ANSYS, Inc. The current in the fiber is nearly uniform over its cross-section; the current density at the center of the fiber is about eight times the current density in the medium. Our goal is to model the same problem via the BEM with a *small* number of basis functions. The set of basis functions to be proposed has been inspired by "rooftop" bases used in high-frequency thin-wire antenna modeling [6]. However, we will use different boundary conditions and a very different charge-to-current relation.

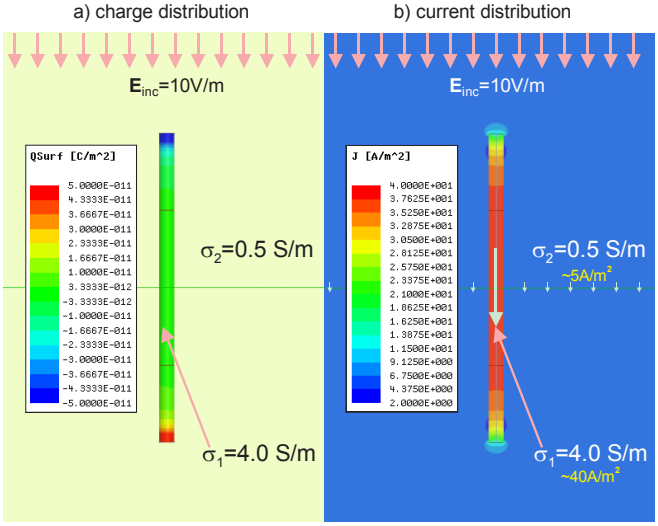

Figure 1. Surface charge and current density distributions for a thin cylinder obtained via FEM modeling – normal incidence.

A. Construction of basis functions – side surface

Consider a situation when the entire *side* surface S of the fiber cylinder is divided into N small unique segments. For every such segment, the surface charge density remains constant. The unknown side surface charge density is expanded into N *doublet* basis functions, $\lambda_n(\mathbf{r})$, defined on two adjacent segments and shown in Fig. 2,

$$\sigma_S(\mathbf{r}) = \sum_{n=1}^{N} a_n \lambda_n(\mathbf{r}) \tag{1}$$

with unknown coefficients, a_n. The doublet basis function can be defined as follows (by analogy with [6])

$$\lambda_n(\mathbf{r}) = \begin{cases} +\dfrac{1}{2\pi a^+ l^+}, & \mathbf{r} \in S^+ \\ -\dfrac{1}{2\pi a^- l^-}, & \mathbf{r} \in S^- \end{cases} \tag{2}$$

where index plus refers to the first tubular segment and index minus – to the second tubular segment; $a^{\pm}$ and $l^{\pm}$ are segment radii and lengths, respectively. A total electric charge supported by every basis function (integral over the surface of two adjacent segments) is exactly *zero*. Every

First author is with the ECE Dept., Worcester Polytechnic Inst., Worcester, MA 01609 (phone: 508-831-5017; fax: 508-831-5491; e-mail: makarov@wpi.edu).

Second author is with Division of Cognitive Neurology, Beth Israel Deaconess Medical Center, Harvard Medical School, Boston, MA 02215.

Third author is with Massachusetts General Hospital, Harvard Medical School, Boston, MA 02114.

978-1-4577-0220-4/16/$31.00 ©2016 IEEE

coefficient a_n has a meaning of the total surface charge per segment (positive or negative) with the units of C.

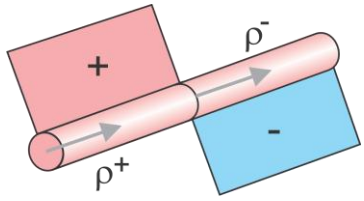

Figure 2. Charge doublet basis function.

Once the solution for fiber charges is known, the corresponding electric potential φ can be found. Then, the electric current density and the total electric current in the fiber can in principle be computed using an expression for the total electric field, $\mathbf{E} = \mathbf{E}_{\text{inc}} - \nabla\varphi$. However, this operation is very time-consuming. In order to find the current for every fiber cross-section, we would need to compute the current density at many separate spatial locations. Instead, we will try to construct the total fiber current associated with every basis function directly. Our solution is based on Gauss' law and current conservation law, respectively. A simplified current flow model is suggested in Fig. 3. Current density inside fiber, $J_1(x)$, is directed along the fiber axis (the *x*-axis) and is uniform over the cross-section. It linearly increases from 0 to a certain maximum value at the joint of two segments. Current density just outside fiber, J_2, is directed along the surface normal vector and is uniform in space.

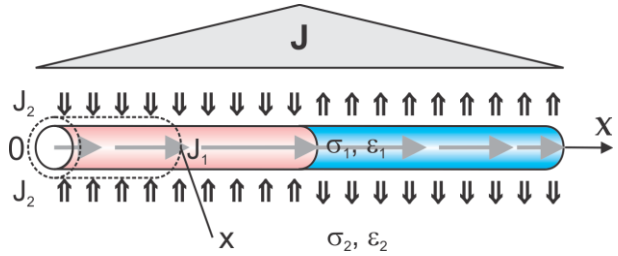

Figure 3. Model of electric current distribution for a single basis function.

For any location *x*, current conservation law for the left segment in Fig. 3 is written in the form

$$\pi a^{+2} J_1(x) = 2\pi a^{+} x J_2 \tag{3}$$

Gauss' theorem for a closed surface indicated by a dashed contour in Fig. 3 yields

$$\pi a^{+2} D_1(x) - 2\pi a^{+} x D_2 = \frac{x}{l^{+}} a_n \tag{4}$$

where *D* is the electric flux density in a medium of interest,

$$D_i = \frac{\varepsilon_i}{\sigma_i} J_i, \quad i = 1,2 \tag{5}$$

With taking into account Eq. (5), a solution to the system of two coupled equations (3), (4) has the form:

$$J_1(x) = \frac{x}{\pi a^{+2} l^{+}} \times \frac{1}{\frac{\varepsilon_1}{\sigma_1} - \frac{\varepsilon_2}{\sigma_2}} \times a_n \tag{6}$$

We introduce vector $\boldsymbol{\rho}^{+}$ drawn from the furthest point of the cylindrical segment labeled plus to the observation point and vector $\boldsymbol{\rho}^{-}$ drawn from the observation point to the furthest point of cylindrical segment labeled minus. The total current ***I*** within the fiber supported by one basis function is thus given by

$$\mathbf{I}(\mathbf{r}) = \boldsymbol{\Lambda}_n(\mathbf{r}) a_n, \quad \boldsymbol{\Lambda}_n(\mathbf{r}) = \begin{cases} \dfrac{\boldsymbol{\rho}^{+}}{l^{+}} \times \dfrac{1}{\frac{\varepsilon_1}{\sigma_1} - \frac{\varepsilon_2}{\sigma_2}}, & \mathbf{r} \in V^{+} \\ \dfrac{\boldsymbol{\rho}^{-}}{l^{-}} \times \dfrac{1}{\frac{\varepsilon_1}{\sigma_1} - \frac{\varepsilon_2}{\sigma_2}}, & \mathbf{r} \in V^{-} \end{cases} \tag{7}$$

$\boldsymbol{\Lambda}_n(\mathbf{r})$ in Eq. (7) is sketched in Fig. 3. It is a familiar vector *rooftop* basis function [6] with *current continuity* at the junction of two segments, which is preserved for non-equal radii. If $\varepsilon_1 = \varepsilon_2 = \varepsilon_0$, $\sigma_1 > \sigma_2$ (which is the present case), then the current in Eq. (7) has a sign *opposite* to the sign of a_n. In other words, it flows from the minus charge to the plus charge of the charge doublet. The total electric current within the fiber is finally obtained in the form

$$\mathbf{I}(\mathbf{r}) = \sum_{n=1}^{N} a_n \boldsymbol{\Lambda}_n(\mathbf{r}) + C \tag{8}$$

Constant *C* is to be defined by an external field, more precisely, by currents entering/leaving the tips of the fiber. Fig. 4 illustrates current/charge expansions into rooftop basis functions (2), (7) for the case when constant *C* in Eq. (8) is equal to zero.

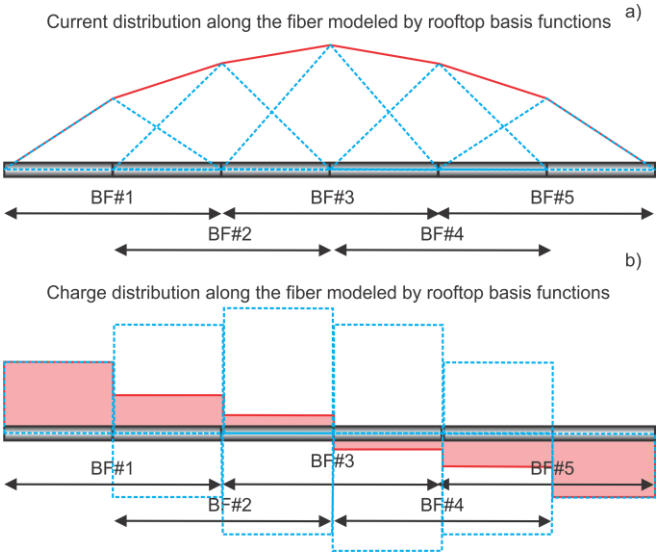

Figure 4. Modeling current and charge distributions with rooftop bases.

B. Construction of basis functions – end cap basis functions

An end-cap basis function is defined for every pair of wire caps. For the surface charge density on caps, one has

$$\sigma_S(\mathbf{r}) = \sum_{n=1}^{N_C} b_n \mu_n(\mathbf{r}) \tag{9}$$

with unknown coefficients, b_n. The corresponding doublet basis function can be defined as follows

$$\mu_n(\mathbf{r}) = \begin{cases} +\dfrac{1}{\pi(a^+)^2}, & \mathbf{r} \in S^+ \\ -\dfrac{1}{\pi(a^-)^2}, & \mathbf{r} \in S^- \end{cases} \quad (10)$$

where $a^{\pm}$ are the radii of two opposite caps. Coefficient b_n has a meaning of the total surface charge per cap with the units of C. There is one such basis function per single wire. Other terminal basis functions have been studied.

C. BEM/MoM Equations

The BEM integral equation for the surface charge density over the entire fiber surface *S* has the standard form [7]

$$\frac{\sigma_S(\mathbf{r})}{2\varepsilon_0} + K\left(\mathbf{n}(\mathbf{r})\cdot\int_S \frac{\sigma_S(\mathbf{r}')}{4\pi\varepsilon_0}\nabla\frac{1}{|\mathbf{r}-\mathbf{r}'|}dS'\right) = K\mathbf{n}\cdot\mathbf{E}_{\text{inc}}(\mathbf{r}) \quad (11)$$

where $K = (\sigma_1 - \sigma_2)/(\sigma_1 + \sigma_2)$ is the conductivity "contrast", $\sigma_{1,2}$ are fiber and medium conductivities, respectively, and **n** is the outer surface normal vector. Using the Bubnov-Galerkin method, we obtain from (11) a system of coupled equations for a_n in (1) and b_n in (9). Double side-to-side, side-to-cap, and cap-to-cap potential integrals of the form

$$\int_{S_n}\int_{S_m} \frac{(\mathbf{r}-\mathbf{r}')\cdot\mathbf{n}(\mathbf{r})}{|\mathbf{r}-\mathbf{r}'|^3} dS'dS \quad (12)$$

must be accurately (pre) computed. To do so, we generally used four uniform numerical interleaving grids (2 linear + 2 angular) of size *M* each, with total M^4 integration points.

III. Modeling Single Straight Fiber

A. Results at normal incident field

We consider the total current distribution along the fiber in Fig. 1 first. Table I reports a relative L^2-norm error percentage between the accurate FEM solution (an adaptively refined mesh with about 2×10^6 tetrahedra has been used) for the total current and the corresponding BEM solution obtained at different sizes of the integration grid, *M*, in Eq. (12). We observe that the accurate computation of the potential integrals is a must for the present BEM solution. In particular, the convergence rate as a function of the number of segments is strongly dependent on the value of *M*.

TABLE I. Relative Error Percentage in Total Current Distrbutioin along the Fiber in Fig. 1.

Integration order, M	Number of segments per fiber				
	5	***10***	***20***	***30***	***40***
11	24.9	16.1	14.5	15.1	15.2
21	19.4	11.5	9.07	9.20	9.20
41	16.7	9.10	5.64	5.38	5.19
61	15.9	8.28	4.42	3.95	3.66
81	15.5	7.88	**3.80**	3.21	2.87

Fig. 5 compares the FEM and BEM solutions for the total fiber current in Fig. 1 when the number of segments along the fiber in the BEM solution is equal to 20. The corresponding error value is marked bold in Table I. We believe that further reduction in the number of segments is possible while maintaining a good accuracy, by using *non-uniform* segment lengths, which would correspond to adaptive BEM mesh refinement [7].

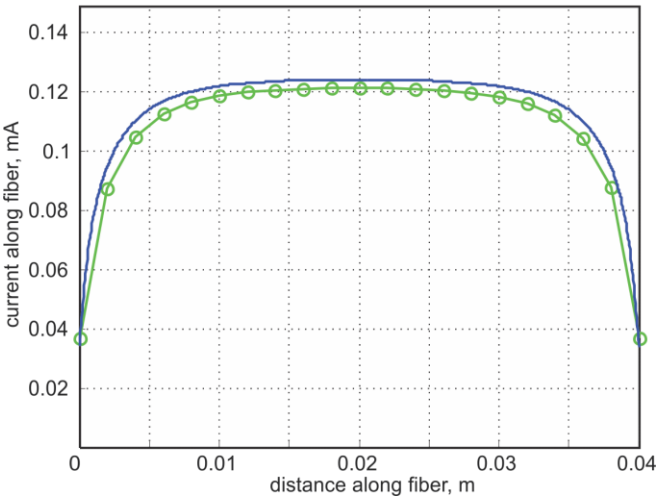

Figure 5. Total current distribution along the fiber in Fig.1b: BEM (circles) versus FEM (solid curve) solutions. The BEM solution uses 20 equal segments.

Table II reports the relative error percentage in the absolute charge (positive charge) over the fiber surface as a function of the number of segment and accuracy of the potential integrals. The FEM total absolute charge is 3.785×10^{-15} C. Note a value marked bold in Table II, which indicates that the error might suddenly jump when potential integrals are computed inaccurately.

TABLE II. Relative Error Percentage in the Absolute Charge (or Positive Charge) over the Fiber Surface in Fig. 1.

Integration order, M	Number of segments per fiber				
	5	***10***	***20***	***30***	***40***
11	16.7	11.0	11.9	13.1	13.5
21	9.47	**33.55**	6.41	7.28	7.50
41	5.62	2.89	2.82	3.38	3.42
61	4.30	1.74	1.46	1.91	1.86
81	3.63	1.14	0.74	1.12	1.03

B. Results at 45 deg incidence

The same cylindrical fiber as in Fig. 1 is considered, but now it is tilted by 45 degrees versus the incident field. FEM simulation results for the surface charge density and current density within the fiber are shown in Fig. 6. This modification might appear trivial from the viewpoint of the one-dimensional BEM theory since only the excitation term in Eq. (11) changes (decreases by $1/\sqrt{2}$). So do the results for the charge and current distributions. However, the FEM solution in Fig. 6a indicates a very non-uniform surface

charge distribution *across* the fiber, which *cannot* be replicated by the one-dimensional model. The same non-uniformity is observed for the electric field *just outside* the fiber. We intend to show that such a distribution has a negligible effect on the total current (and essentially on the current density inside the fiber) in any fiber's cross-section and on the absolute value of the net positive charge. To do so, Table III reports a relative L^2-norm error percentage between the accurate FEM solution (an adaptively refined mesh with about 2×10^6 tetrahedra has been used again) for the total current and the corresponding BEM solution obtained at different sizes of the integration grid, M, in Eq. (12). We observe nearly the same (and perhaps even slightly better) convergence rate as compared to Table I.

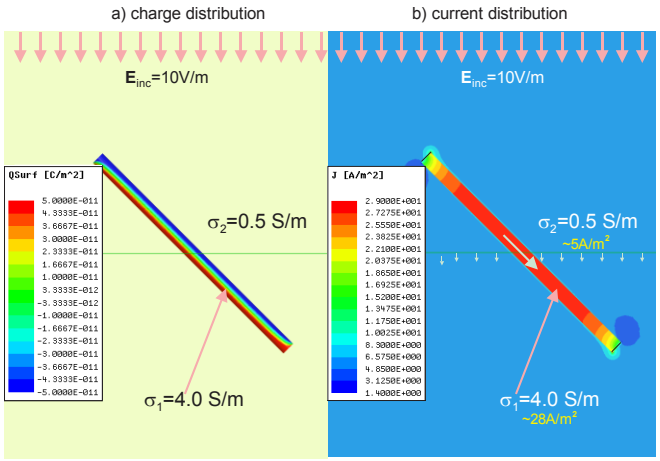

Figure 6. Surface charge and current density distributions for a thin cylinder obtained via FEM modeling – 45 deg. incidence.

TABLE III. RELATIVE ERROR PERCENTAGE IN TOTAL CURRENT DISTRBUTIOIN ALONG THE FIBER IN FIG. 6.

Integration order, M	Number of segments per fiber				
	5	*10*	*20*	*30*	*40*
11	24.8	16.0	14.5	15.0	15.1
21	19.3	11.5	8.98	9.11	9.11
41	16.7	9.04	5.56	5.29	5.09
61	15.9	8.22	4.34	3.86	3.57
81	15.5	7.82	**3.73**	3.12	2.78

Fig. 7 compares the FEM and BEM solutions for the total fiber current in Fig. 6 when the number of segments along the fiber in the BEM solution is equal to 20. The corresponding error value is marked bold in Table III. Table IV reports the relative error percentage in the absolute charge (positive charge) averged over the tube cross-section and then integrated over the entire fiber surface as a function of the number of segment and accuracy of the potential integrals. The corresponding FEM total charge value is 2.74×10^{-15} C.

IV. CONCLUSIONS

We have constructed and tested the one-dimensional MoM basis functions (rooftop basis functions) applicable to modeling thin highly conducting cylindrical fiber-like objects embedded into a low-conductivity medium. A direct-current problem has been considered. The ultimate goal of this study is to apply the model to the large-scale bundles of axonal fibers in the human brain.

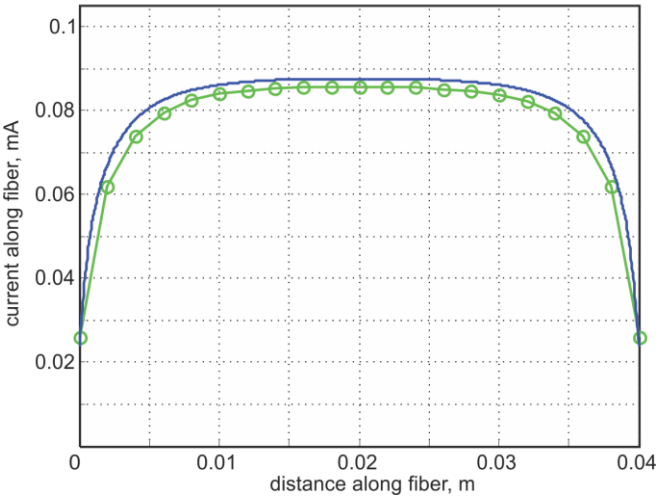

Figure 7. Total current distribution along the fiber in Fig.6b: BEM (circles) versus FEM (solid curve) solutions. The BEM solution uses 20 equal segments.

TABLE IV. RELATIVE ERROR PERCENTAGE IN THE ABSOLUTE CHARGE (OR POSITIVE CHARGE) OVER THE FIBER SURFACE IN FIG. 6.

Integration order, M	Number of segments per fiber				
	5	*10*	*20*	*30*	*40*
11	18.6	13.0	14.0	15.1	15.5
21	11.6	8.21	8.58	9.43	9.64
41	7.80	5.14	5.07	5.62	5.66
61	6.52	4.02	3.75	4.18	4.13
81	5.86	3.43	3.05	3.42	3.33

REFERENCES

[1] M. Hämäläinen *et al.*, "Magnetoencephalography—theory, instrumentation, and applications to noninvasive studies of the working human brain," *Reviews of Modern Physics*, vol. 65(2), pp. 413-497, April 1993.

[2] A. Nummenmaa *et al.*, "Targeting of White Matter Tracts With Transcranial Magnetic Stimulation," *Brain Stimulation*, pp. 1-5, 2013.

[3] M. Bikson *et al.*, "High-resolution modeling assisted design of customized and individualized transcranial direct current stimulation protocols," *Neuromodulation*, vol. 15(4), pp. 306-315, 2012.

[4] A. Datta *et al.*, "Gyri -precise head model of transcranial DC stimulation: Improved spatial focality using a ring electrode versus conventional rectangular pad," *Brain Stimulation*, vol. 2(4), pp. 201-217, 2009.

[5] A. Nummenmaa *et al.*, "Comparison of spherical and realistically shaped boundary element head models for transcranial magnetic stimulation navigation," *Clinical Neurophysiology*, vol. 214(10), pp. 1995-2007, 2013.

[6] A.W. Glisson, S. M. Rao, and D. R. Wilton, "Physically-based approximation of electromagnetic field quantities," (Invited) *Proceedings of the 2002 IEEE Antennas and Propagation Society International Symposium*, pp. 78-81, San Antonio, June 2002.

[7] S. N. Makarov, G. Noetscher, and A. Nazarian, *Low-Frequency Electromagnetic Modeling for Electrical and Biological Systems Using MATLAB*, Wiley, NY, July 2015.